

To appear in *Liquid Crystals*  
Vol. 00, No. 00, Month 20XX, 1–10

## RESEARCH ARTICLE

# Solvent-induced self-assembly of uniform lying helix alignment of the cholesteric liquid crystal phase for the flexoelectro-optic effect

S. Bolis<sup>a,b,c\*</sup>, C.C. Tartan<sup>c</sup>, J. Beeckman<sup>b</sup>, P. Kockaert<sup>a</sup>, S.J. Elston<sup>c</sup>, and S.M. Morris<sup>c\*\*</sup>

<sup>a</sup> *Université libre de Bruxelles, OPERA-Photonics Group, 50 Avenue F.D.Roosevelt CP 194/5 1050 Bruxelles Belgium;* <sup>b</sup> *Gent Universiteit, ELIS Department, Technologiepark-Zwijnaarde 15, 9052 Gent Belgium;* <sup>c</sup> *University of Oxford, Department of Engineering Science, Parks Road, Oxford OX1 3PJ United Kingdom*

(v2.1 released January 2014)

A uniform lying helix (ULH) alignment of cholesteric liquid crystals (CLCs) is obtained using a solvent evaporation technique. The solvent evaporation method allows for the spontaneous formation of a virtually defect-free alignment, even in the absence of an external electric field. The small amount of solvent diffuses into the LC and changes its phase into the isotropic state where the individual LC molecules are more mobile. As the solvent diffuses out of the LC and consequently evaporates, additional mobility provided by the solvent allows the molecules to reach the lowest energy configuration, dictated by the boundary conditions, the solvent evaporation direction and the elastic forces among the molecules. Compared to a shear-flow-induced alignment, the solvent-induced ULH exhibits a contrast ratio between the bright and dark states that is a factor of 4 greater, due to the low number of defects in the structure. From measurements of the flexoelectro-optic effect, the difference between the splay and bend flexoelectric coefficients,  $e_1 - e_3$ , for the nematic LC E7 is found to be in agreement with the measured values reported in the literature ( $12.1 \pm 1.0$  pC/m), demonstrating that the solvent self-aligning does not change the electric response of the medium, while improving its optical properties.

**Keywords:** solvent-induced self-alignment, flexoelectro-optic effect, uniform lying helix, cholesteric liquid crystals

## 1. Introduction

Flexoelectro-optic switching is a fast in-plane rotation of the optic axis that can be observed in cholesteric liquid crystals (CLCs) when an electric field is applied perpendicular to the helix axis [1–3]. The uniform lying helix (ULH) alignment of CLCs is of particular interest for flexoelectro-optic switching as it does not require an in-plane electric field, which typically necessitates the use of interdigitated electrodes that can result in highly non-uniform electric fields. As the response times can be sub-millisecond, this opens up the possibility of realizing frame sequential color in next generation flat panel displays and is also important for other fast-switching photonics applications [4]. However, despite the obvious benefits of a ULH configuration, achieving a high quality alignment still remains a challenge [5–7].

With methods involving external electric fields and shear flow, it is extremely difficult to obtain a ULH with high optical contrast between the dark and bright states. To date, a number of techniques have been considered to induce a ULH alignment: for example, shear flow through the application of mechanical stress to the glass substrates [5], the application of an electric field with [6] or without [8] thermal cycling, bespoke surface anchoring conditions [9, 10], periodic structured templating [11,

---

\*Corresponding author. Email: serena.bolis@ulb.ac.be

\*\*Corresponding author. Email: stephen.morris@eng.ox.ac.uk

12] and, recently, polymer network structuring by two-photon photo-polymerization [13]. Even though many of these reports have shown promising results, such techniques either require complex fabrication procedures to form the lying helix alignment or they result in a relatively low optical contrast between the bright and dark states.

In this work, we show that a solvent evaporation technique applied to a CLC can result in the formation of a high quality ULH configuration. Solvent evaporation methods have been widely studied as an effective way of self-aligning patterns of nanoparticles: the solvent screens the weak forces among the nanoparticles that slowly start to interact as the solvent evaporation process begins [14–22]. In those systems, the interaction force among the particles is stronger than the thermal fluctuations, but, at the same time, weak enough to allow the system to reach the lowest energy equilibrium configuration [17, 21]. The weak interactions among the nanoparticles drive the self-assembly and they can be of different origins, ranging from van der Waals attraction to electrostatic interactions and hydrogen bonding [18].

The self-assembled structures can be of one-, two- and three-dimensions [15, 21, 23]. The packing, and therefore the type of lattice, can be determined by the shape of the nanoparticles [15], the interactions among the nanoparticles [15, 24] and by the boundary conditions that are used in the growth process [25]. The evaporation rate determines the regularity of the structure [26, 27], while the choice of the solvent can change the interaction amongst the nanoparticles, inducing aggregates or uniform layers [28, 29]. Finally, by carefully choosing the geometry of the sample, it is possible to control the direction of evaporation and therefore the direction of the growth of the lattice [25, 30].

In this paper, we apply this technique to LCs, in particular to obtain a highly defect-free ULH alignment. In our case the interactions among the nanoparticles are replaced by the weak elastic forces among the LC molecules. The highly uniform and virtually defect-free ULH texture that is obtained using this approach exhibits a larger contrast ratio than is typically observed using conventional alignment procedures, with the advantage that no external stimulus is needed to obtain the alignment. Even though these regions are only a few hundreds of  $\mu\text{m}$  across, they can be of interest for applications such as thin film lasers [31] and spatial light modulator technology [32], where small high-quality areas of alignment are required.

## 2. Solvent-induced ULH self-alignment

The cells are fabricated by assembling two glass plates that are spin-coated with the homeotropic alignment layer SE4811 (Nissan). The LC layer thickness is defined by 10  $\mu\text{m}$  spacers. A thin ( $\sim 100$   $\mu\text{m}$ ) glass plate coated with a planar alignment layer (rubbed Nylon 6,6) is then glued onto one edge of the cell (Inset of Fig.1). The glue is mixed with 3  $\mu\text{m}$  spacer beads, in order to prevent a complete filling of the cell gap when gluing the side glass. The glue distribution on the side glass window is arranged so that it is not continuous, but instead consists of gaps to allow for a relatively slow and directional evaporation of the solvent. Finally, to add mechanical stability to the side glass wall, a highly viscous glue (Norland Optical Adhesive 68T) is used to fix the side window.

The cells are then filled with a CLC mixture consisting of 3.86%wt BDH1281 chiral dopant (Merck KGaA) in the commercially available nematic LC mixture, E7 (Synthon). The mixture exhibits a reflection band in the range 530 nm - 605 nm and, consequently, a pitch of  $\sim 350$  nm. Two kinds of ULH alignments are grown in the same glass cell. A shear flow induced ULH is formed by heating the sample above the clearing temperature (62  $^{\circ}\text{C}$ ). The cell is then slowly cooled in the presence of a voltage of  $\pm 5$  V at 1kHz while mechanically shearing the cell to induce an oscillatory flow. The electric field promotes the ULH over the standing helix alignment (Grandjean texture) while the shear flow establishes the orthogonality of the helix axis relative to the direction of the flow. [5]

The solvent-induced ULH is grown by depositing a small quantity (few  $\mu\text{l}$ ) of acetone onto the entrance/opening of the cell which was pre-filled with the CLC mixture. The small amounts of

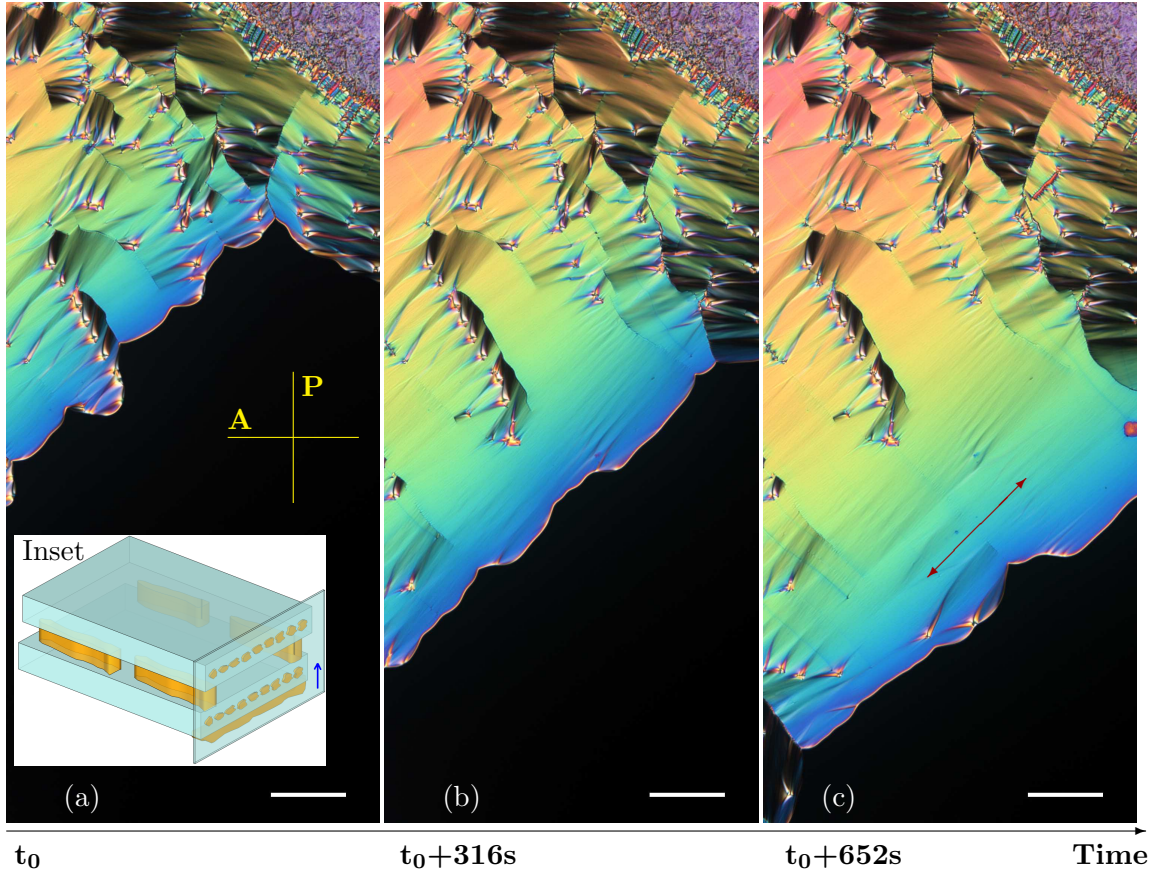


Figure 1. (Color online) Inset: arrangement of the LC cell (not in scale), formed from two thick glass plates coated with homeotropic alignment layer, together with a thin side window coated with planar alignment (the blue arrow indicates the rubbing direction). The glue is distributed along the edges and also a highly viscous glue is used at the bottom side of the side window. (a)-(c) Polarized optical microscopy (POM) images of the formation of the ULH alignment over time. The black areas are the isotropic regions induced by the acetone, while the rainbow colors in the ULH are due to a birefringence gradient dictated by an increasing concentration of acetone towards the black region. The red arrow indicates the helix axis orientation (scale bar: 100  $\mu\text{m}$ ).

acetone that enters the cell by capillary action is not enough to displace the LC from the cell but instead it diffuses into the LC, in a sufficient quantity to cause a transition from the liquid crystalline to the isotropic state. In Fig.1, it is possible to observe the as-filled CLC texture that is not directly influenced by the solvent (top right of Fig.1), together with the interface between the isotropic state (larger concentration of acetone, black region) and the LC state (low concentration of acetone, colored region). The color sequence adjacent to the black isotropic region towards the center of the cell is indicative of an increase in the birefringence. This arises due to a gradient in the diffusion of the acetone inside the cell and a consequent gradient of the LC concentration in the direction of the diffusion. Due to the confinement provided by the two glass plates forming the cell, the acetone gradually evaporates from the edge of the cell. Depending upon the region we are looking at, the solvent can evaporate from the side window or from the open entrance of the cell. The evaporation process leads to a progression in the acetone concentration gradient and is therefore visualized by the progress of the colors over time.

Only a very small flow of the LC is associated with this process. In fact, flow alignment, and similarly diffusion, both tend to align CLCs with their helical axis perpendicular to the flow direction because flow/diffusion along the helical axis is hindered [5].

A way to evaluate the importance of the flow-induced alignment is the Ericksen number [33]

$$Er = \frac{\eta v L}{K} \quad (1)$$

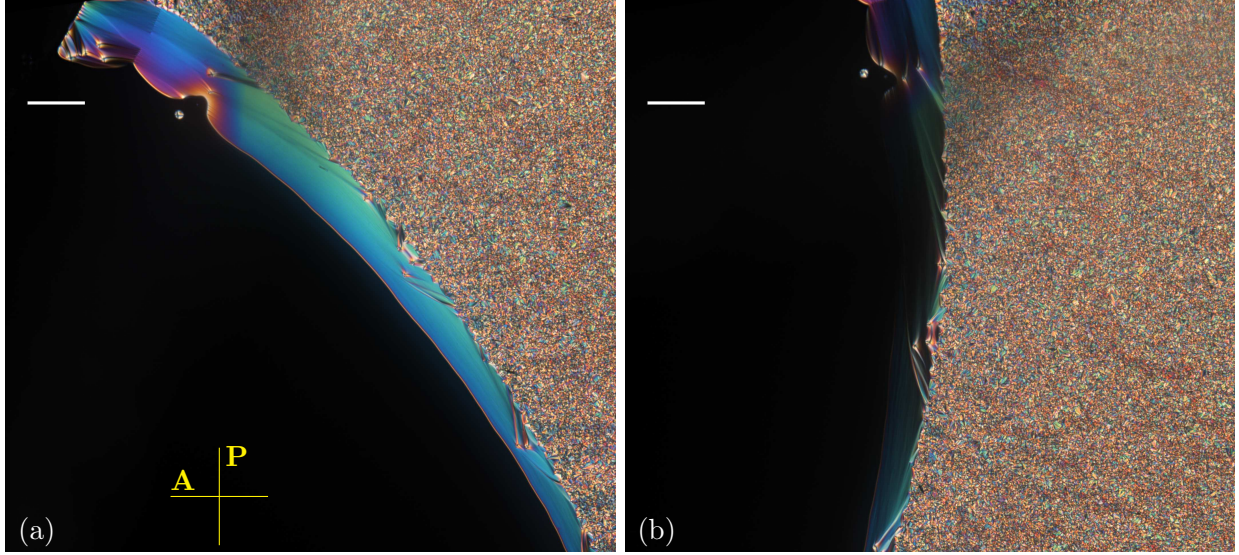


Figure 2. (Color online) POM images of the bright (a) and dark (b) states of the solvent-induced ULH growth in the case where the diffusion/evaporation is not unidirectional. The helix axis is parallel to the curved front between the isotropic and LC phases (scale bar: 100  $\mu\text{m}$ ).

where  $\eta$  is the viscosity of the LC ( $\eta=0.08$  Pa·s for E7 [34]),  $v$  is the flow velocity ( $v \simeq 0.6 \times 10^{-6}$  m/s, extracted from the image sequence shown in Fig.1),  $L$  is the characteristic length scale of the system ( $L = 10$   $\mu\text{m}$ , the thickness of the cell) and  $K$  is the highest of the three elastic constants of the LC ( $K_3 = 16$  pN [6]). With these values, we obtain  $Er \simeq 0.03 \ll 1$ , indicating that the effect of flow is probably insignificant for the alignment of the LC in our case [33]. Also note that we take for  $v$  the velocity of the phase transition front, which is only the upper bound for the actual LC velocity, so the flow effect is likely to be rather small. Indeed, the few defects which are present in regions where the ULH has formed do not change position whilst the birefringence colors change as the acetone diffuses from the cell, indicating that the acetone concentration is low and it slowly decreases without significant flow of the LC. However, any degree to which the flow does contribute to the alignment, is also such that the helix axis would form parallel to the evaporation front. From Fig.1 it is possible to see that the ULH texture is formed over the course of several minutes. However, the slow color progression indicates that an amount of solvent may remain in the sample. Therefore, for this reason we left the solvent to completely evaporate (and the cell to acquire a uniform color) over a period of two days before the device characterization was carried out.

Due to the slow evaporation rate of the acetone coupled with the high mobility of the LC molecules in the solvent-induced isotropic state, the LC molecules at the isotropic/nematic interface are able to rearrange themselves in a lower energy configuration, which is dictated by the chirality of the mixture, the spin-coated homeotropic surface on the two glasses and the homeotropic alignment at the interface with the acetone (a polar solvent) [35]. For these reasons, the helix is lying in the plane of the cell at the interface, with its axis parallel to the evaporation boundary. The orientation of the helix axis has been verified with a Berek compensator.

In Fig.2 we show that, when the evaporation/diffusion process takes place far from the side window, the isotropic-nematic interface front can be curved and the helix axis orientation follows the shape of the phase-transition front. It is also possible to see that the ULH alignment is reached independently of the initial conditions of the LC alignment (focal conic texture in our case, as can be seen in the right part of the Fig.2). Indeed, the LC self-assembly, starting from an isotropic-like phase where the LC molecules are randomly oriented in the solvent, is only dictated by the interaction among the molecules, the boundary conditions and the direction of the solvent diffusion. It is for this reason that the side glass mentioned above was added to the cell, in order to control



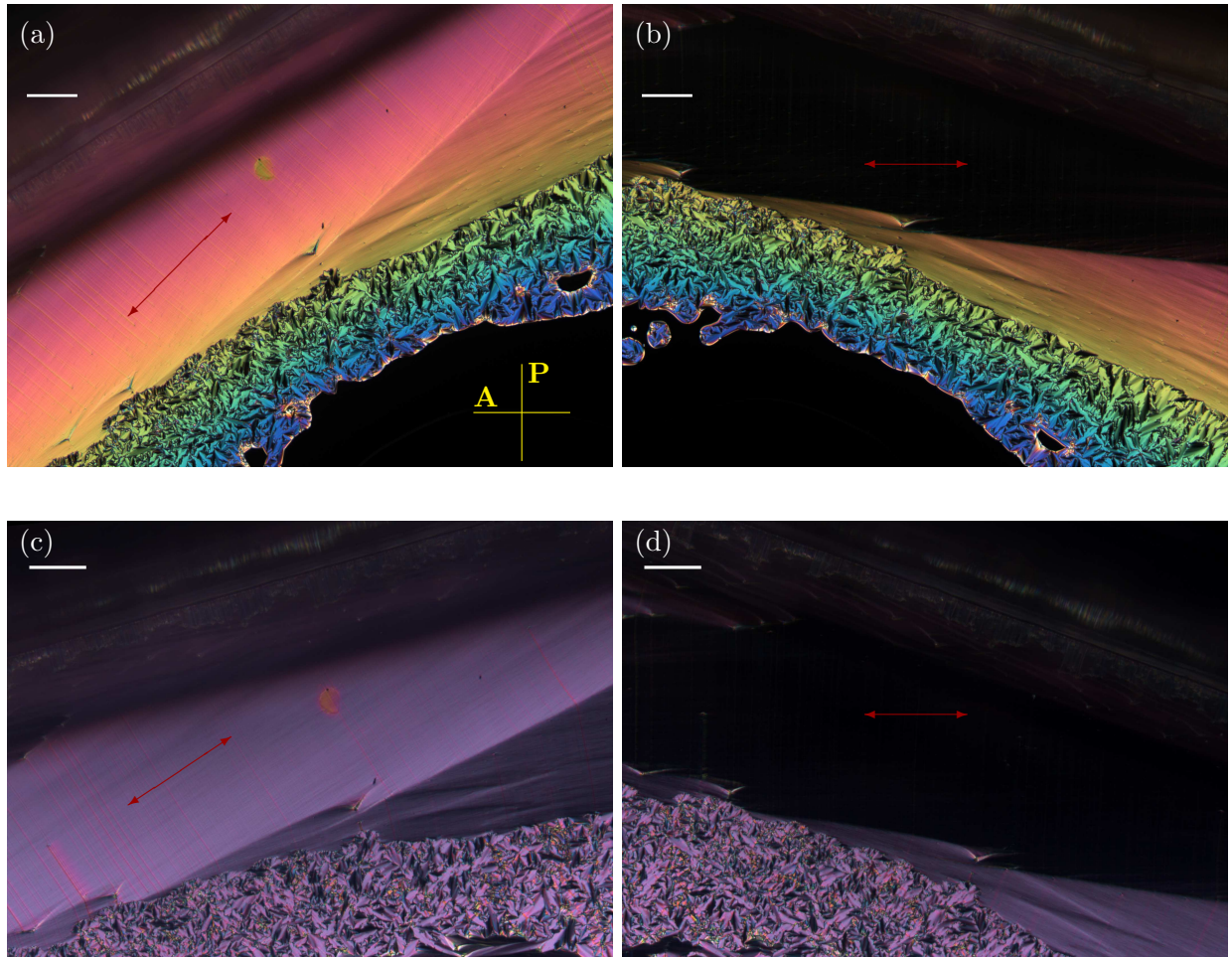


Figure 3. (Color online) Polarized optical microscopy images of the bright (a),(c) and dark (b),(d) states of the solvent-induced ULH growth in the case where the diffusion and evaporation is controlled by the side window. The color sequence, indicating a gradient of the birefringence, is present during the solvent diffusion and evaporation (a),(b), while a uniform sample is obtained when no acetone is left in the sample (c),(d). The ghost image in the upper part of the figures is due to the reflection from the side glass window, while the glue used to fix the glass also leads to a blurry dark shadow close to the edge. The red arrow indicates the helix axis orientation (scale bar: 100  $\mu\text{m}$ ).

the solvent evaporation and hence diffusion direction within the cell.

In Fig. 3 we show the result of the self-assembly close to the side window, before (a-b) and after (c-d) the complete evaporation of the solvent. In this region the highly homogeneous ULH alignment extends over several hundreds of  $\mu\text{m}$ . Its extent is only limited by the fact that, after initial evaporation of the solvent close to the edge, the acetone tends to be trapped in the central region of the cell, where it tends to diffuse in all directions at the same time, generating the rather scrambled alignment texture visible in the lower region of the images. Close to the edge of the device, the evaporation/diffusion is almost unidirectional and the ULH grows into much larger homogeneous regions (Fig. 3). Indeed, the diffusion direction is orthogonal (or close to orthogonal) with respect to the side window. The almost flat front of the phase transition then causes the helix axis orientation to be homogeneous over large regions.

### 3. Optical characterization

In order to show the optical quality of the solvent-induced ULH alignment, we compare it to the shear-flow-induced ULH. In Fig.4 we show the bright (a,d) and dark (b,e) states for the respective

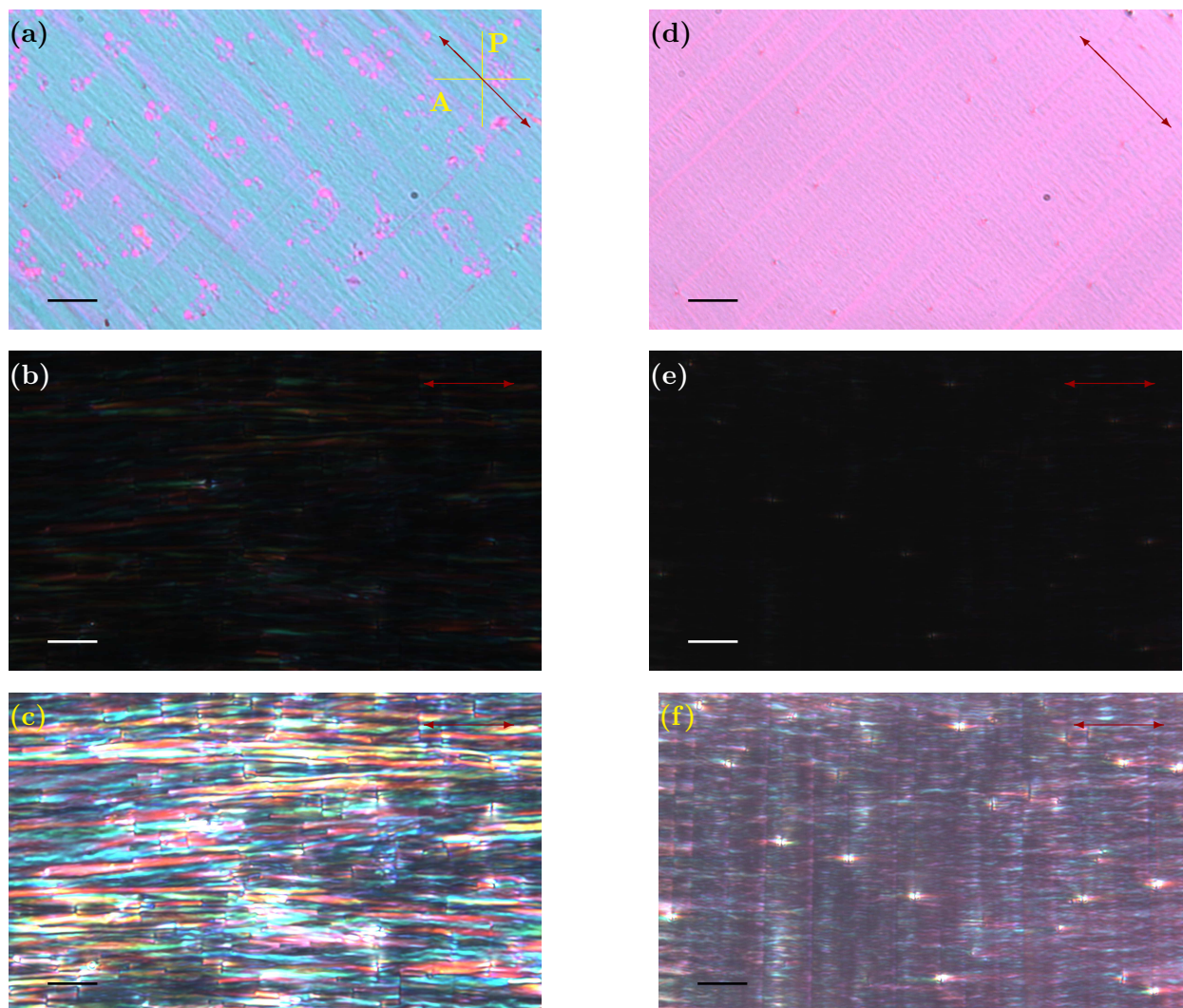


Figure 4. (Color online) POM images of the bright and dark states for the shear-flow (a)-(c) and solvent (d)-(f) induced ULH alignment. (c),(f) are enhanced brightness images of the dark states. The red arrow indicates the helix axis orientation (scale bar: 20  $\mu\text{m}$ ).

shear-flow and solvent-induced ULH alignments. The solvent-induced sections are taken in the region toward the side window showed in Fig.3. The bright state of the shear-flow-induced ULH exhibits some striping in the direction of the helix axis, which is comparatively non-existent in the solvent-induced alignment. Enhancing the acquisition time of the camera (Fig.4c,f), it is possible to visualise the defects in the dark state images, where the elongated domains from the shear flow case are much more evident, and the homogeneous texture for the solvent case is highlighted. Some defect points of a few  $\mu\text{m}$  in diameter are still visible in the solvent-induced ULH, but the improvement in the alignment is evident.

In order to quantify the quality of the ULH texture, we measured the contrast ratio ( $CR$ ) defined as the ratio of the intensity of the bright state to the intensity of the dark state. The intensity is averaged over an area of around  $100 \mu\text{m}^2$  and, for both the dark and the bright state, the dark level for the camera is subtracted. The  $CR$  was measured with a broad-spectrum white light source focused on the sample with the condenser of the microscope set to a N.A. of 0.8 and collected with a 50x objective (Nikon, N.A.=0.7). For the shear flow case, a large amount of micro-domains can be seen in Fig.4. The difference in the orientation of the optic axis between each sub-domain leads to optical scattering that degrades the overall quality of the dark state, resulting in a  $CR$  of  $\approx 30$ .

However, for the solvent-induced ULH alignment case we obtain a  $CR$  of  $\approx 120$ , on account of the largely defect-free structure that results from the latter technique. For this reason, the  $CR$  increases by a factor of four for the solvent-induced case, demonstrating the higher quality of the ULH alignment. For comparison, using the same measurement technique, the  $CR$  for a planar nematic E7 device of  $5\text{ }\mu\text{m}$  thickness was found to be  $\approx 160$ . Therefore, the contrast ratio of the solvent-induced ULH aligned device is approaching that of a planar aligned nematic device with a similar optical retardation.

## 4. Flexoelectro-optic response

### 4.1 Experiment

A square-wave electric field is applied to the LC cell to characterize the flexoelectro-optic response. For small angles, the tilt of the optic axis induced by the flexoelectro-optic response is a near-linear function of the amplitude of the electric field and, for the case of a helix pitch fixed at the natural pitch  $p$ , it follows the relation [3, 36]

$$\tan \phi = \frac{p}{2\pi} \frac{(e_1 - e_3)}{2K_2} E - \frac{K_1 - 2K_2 + K_3}{2K_2} \sin \phi, \quad (2)$$

where  $\phi$  is the tilt angle of the optic axis with respect to the helix axis,  $E$  is the magnitude of the applied electric field,  $K_1$ ,  $K_2$  and  $K_3$  are the splay, twist and bend elastic coefficients, respectively, and  $e_1$  and  $e_3$  are the splay and bend flexoelectric coefficients, respectively.

The reorientation angle due to the flexoelectro-optic response is measured using a standard technique. [9, 13] The cell is placed on the microscope with the collected transmitted light passing to a photo-diode to measure the intensity of the light transmitted by the cell. Since the pitch of the ULH is shorter than the wavelength of visible light, the ULH layer acts as an optically uniaxial material. The transmission is therefore described by  $T = T_{max} \sin^2(2\chi)$ , where  $\chi$  is the angle between the ULH field-dependent optical axis and the transmission axis of one of the polarizers, and  $T_{max}$  is the difference in transmission between the bright and the dark states. Then, the ULH is placed with the helix axis at  $22.5^\circ$  from the polarizer axis, in the linear regime of the transmission response, where the amplitude  $\Delta\chi$  of small fluctuations in the optic axis orientation angle is related to the amplitude  $\Delta T$  of the modulated transmission through the relation  $\Delta\chi = \Delta T / (2T_{max})$ . A square wave of amplitude  $E$  is applied to the cell, and after an equilibrium is reached, the modulated transmitted intensity for the reorientation of the ULH is recorded (Fig.5a). From the measurement of the amplitude of the modulation we can obtain the reorientation angle  $\Delta\chi$ , which is the electric field dependent tilt angle  $\phi$  in Eq.(2).

### 4.2 Results

Both the shear-flow-induced and solvent-induced ULH alignment exhibit a flexoelectro-optic response when an a.c. electric field is applied (Fig.5). The temporal dynamics of the transmitted intensity for both ULH states is shown in Fig.5a. For low voltages, both textures tend to show the same dynamic behaviour, while, for higher voltages, we observe a drop in the response for the solvent-induced alignment. The response time, defined as the time required for the transmission to increase from 10% to 90%, decreased from  $70\text{ }\mu\text{s}$  to  $50\text{ }\mu\text{s}$  when the electric field increased from  $1.5\text{ V}/\mu\text{m}$  to  $5\text{ V}/\mu\text{m}$  for both textures. From the amplitudes of the data shown in Fig.5a we can extract the tilt angle  $\phi$  as a function of the electric field as explained above. Fitting Eq.2 to our data, it is possible to find the value for the flexoelectric difference  $e_1 - e_3$  that provides the best-fit, as shown in Fig.5b-c. Using the values  $K_1 = 10.7\text{ pN}$ ,  $K_2 = 6.5\text{ pN}$  and  $K_3 = 16.0\text{ pN}$  for E7 [6] and  $p = 350\text{ nm}$ , we obtain  $e_1 - e_3 = 12.1 \pm 1.0\text{ pC/m}$  for both the shear-flow-induced



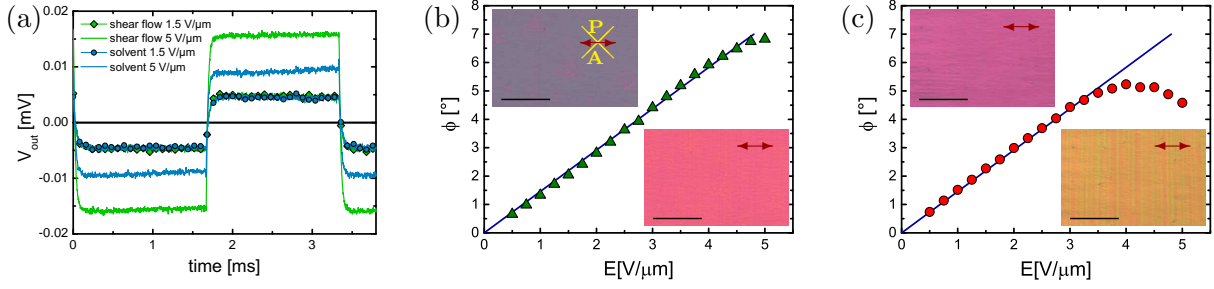


Figure 5. (Color online) (a) Temporal dynamics of the transmitted light through the ULH CLC between two crossed polarisers, for both types of alignment at two different voltages. (b)-(c) Experimental values (symbols) and fit based on Eq.(2) (line) of the tilt angle of the optic axis as a function of electric field for the shear-flow (b) and the solvent (c) induced ULH. The frequency of the square-wave electric field is 300 Hz. Insets: POM images of the alignment at  $E = 2.5$  V/μm (top left) and  $E = 5.0$  V/μm (bottom right) for the shear-flow (b) and the solvent (c) induced ULH; the red arrow indicates the helix axis orientation (scale bar: 50 μm).

and solvent-induced alignment, indicating that no solvent or impurities are left in the sample, as this would tend to influence the flexoelectro-optic response. Also, the value for  $e_1 - e_3$  is in good agreement with the values reported in the literature [6, 9]. Increasing the field amplitude, the tilt angle of the shear-flow-induced ULH remains approximately linear over the entire electric field regime considered here, with a small deviation at 5 V/μm. The shear-flow-induced ULH texture also appears to remain homogeneous for all field strengths (insets Fig.5b).

On the other hand, the tilt angle for the solvent-induced ULH deviates substantially from linear behaviour for electric fields greater than around 4 V/μm. Interestingly, above this field strength, defect lines are observed propagating orthogonal to the helix axis (insets Fig.5c). Of course, some distortion in the helix may be expected for applied fields approaching the critical field  $E_c$  [37]. However, importantly, here we appear to observe unwinding taking place through the propagation of the defect lines for fields greater than around 4 V/μm. The critical field for the unwinding of the helix, including the flexoelectric contribution, is given by [4]

$$E_c = \frac{\pi^2}{p_0} \sqrt{\frac{K_2}{\varepsilon_0 \Delta\varepsilon - \frac{\pi^2(e_1 - e_3)^2}{16(K_1 + K_3)}}} \quad (3)$$

where  $\varepsilon_0$  is the permittivity of free space and  $\Delta\varepsilon$  is the dielectric anisotropy. For E7 [6] we have  $\Delta\varepsilon = 13.7$ , which together with the value of  $e_1 - e_3$  we have determined, gives a value for the critical electric field of  $E_c = 6.9$  V/μm.

When the applied electric field approaches this value, the constrained pitch of the helix is somewhat different from its equilibrium value. There is therefore a tendency for the helix pitch to change through an unwinding process. In principle, two unwinding mechanisms are possible, one where the pitch changes continuously, and one where the pitch changes discontinuously (through defect formation/growth). In general, we do not expect the first of these to take place in ULH devices due to surface and bulk helix pinning interactions. However, helix unwinding through defect formation/growth is possible. Interestingly, we observe this to be much more prevalent in the high quality solvent-induced ULH alignment (inset of Fig.5c) than in the lower quality shear-flow-induced alignment. It therefore appears that the high concentration of domain edges in the latter case tends to block the growth of the unwinding lines (i.e. growth of defects and dislocations are pinned). In the unwound portions of the helix, the dielectric interaction tends to suppress the flexoelectro-optic tilt angle and therefore we observe a drop in the electro-optic response at higher fields for the solvent-induced ULH alignment where significant helix unwinding takes place (Fig.5c). This indicates that in practice structural stabilization, using for example a polymer network, would be very important to ensure electric field-stability of the solvent-induced ULH structure [13]. This is currently under study.



## 5. Conclusions

In summary, we have demonstrated how a solvent-induced self-assembly technique can be applied to LC alignments. The slow and directional diffusion/evaporation of the solvent allows the system to reach the minimal energy configuration, which corresponds to the ULH state in our case. The ULH obtained with this technique exhibits an extremely homogeneous alignment that translates into a high optical quality and a large contrast ratio. The flexoelectro-optic response shows that the technique does not alter the electric response (at low fields), while increasing the optical quality of the alignment. We believe that this technique could provide new opportunities for defect-free self-assembly of LC textures and phases, with particular interest for templated and structured devices, where LC defects are difficult to avoid.

## Funding

We thank the Belgian Science Policy Office (BELSPO) (IAP7-35), the Engineering and Physical Sciences Research Council (UK) through the project EP/M017923/1, the Fondation Philippe Wiener - Maurice Anspach, the Fund for Research Training in Industry and Agriculture (FRIA), the Fonds David et Alice Van Buuren and the Fondation Jaumotte-Demoulin, Merck Chemicals Ltd for a studentship and The Royal Society (London, UK).

## References

- [1] Patel JS, Meyer RB. Flexoelectric electro-optics of a cholesteric liquid crystal. *Phys Rev Lett.* 1987; 58(15):1538.
- [2] Patel J, Lee SD. Fast linear electro-optic effect based on cholesteric liquid crystals. *J Appl Phys.* 1989; 66(4):1879–1881.
- [3] Rudquist P, Carlsson T, Komitov L, Lagerwall S. The flexoelectro-optic effect in cholesterics. *Liq Cryst.* 1997;22(4):445–449.
- [4] Coles HJ, Morris SM. Flexoelectro-optic liquid crystal displays. *Handbook of Visual Display Technology.* 2012;:1681–1694.
- [5] Inoue Y, Moritake H. Formation of a defect-free uniform lying helix in a thick cholesteric liquid crystal cell. *Appl Phys Express.* 2015;8(7):071701.
- [6] Salter P, Kischka C, Elston S, Raynes E. The influence of chirality on the difference in flexoelectric coefficients investigated in uniform lying helix, grandjean and twisted nematic structures. *Liq Cryst.* 2009;36(12):1355–1364.
- [7] Coles HJ, Clarke MJ, Morris SM, Broughton BJ, Blatch AE. Strong flexoelectric behavior in bimesogenic liquid crystals. *J Appl Phys.* 2006;99(3):034104.
- [8] Gardiner DJ, Morris SM, Hands PJ, Castles F, Qasim MM, Kim WS, Choi SS, Wilkinson TD, Coles HJ. Spontaneous induction of the uniform lying helix alignment in bimesogenic liquid crystals for the flexoelectro-optic effect. *Appl Phys Lett.* 2012;100(6):063501.
- [9] Outram B, Elston S. Spontaneous and stable uniform lying helix liquid-crystal alignment. *J Appl Phys.* 2013;113(4):043103.
- [10] Carbone G, Corbett D, Elston SJ, Raynes P, Jesacher A, Simmonds R, Booth M. Uniform lying helix alignment on periodic surface relief structure generated via laser scanning lithography. *Mol Cryst Liq Cryst.* 2011;544(1):37–1025.
- [11] Carbone G, Salter P, Elston SJ, Raynes P, De Sio L, Ferjani S, Strangi G, Umeton C, Bartolino R. Short pitch cholesteric electro-optical device based on periodic polymer structures. *Appl Phys Lett.* 2009;95(1):011102.
- [12] Caputo R, De Luca A, De Sio L, Pezzi L, Strangi G, Umeton C, Veltri A, Asquini R, d'Alessandro A, Donisi D. Polycryps: a liquid crystal composed nano/microstructure with a wide range of optical and electro-optical applications. *J Opt A: Pure Appl Opt.* 2009;11(2):024017.

- [13] Tartan CC, Salter PS, Booth MJ, Morris SM, Elston SJ. Localised polymer networks in chiral nematic liquid crystals for high speed photonic switching. *J Appl Phys.* 2016;119(18):183106.
- [14] Bigioni TP, Lin XM, Nguyen TT, Corwin EI, Witten TA, Jaeger HM. Kinetically driven self assembly of highly ordered nanoparticle monolayers. *Nat Mater.* 2006;5(4):265–270.
- [15] Sau TK, Murphy CJ. Self-assembly patterns formed upon solvent evaporation of aqueous cetyltrimethylammonium bromide-coated gold nanoparticles of various shapes. *Langmuir.* 2005;21(7):2923–2929.
- [16] Ohara PC, Leff DV, Heath JR, Gelbart WM. Crystallization of opals from polydisperse nanoparticles. *Phys Rev Lett.* 1995;75(19):3466.
- [17] Tang J, Ge G, Brus LE. Gas- liquid- solid phase transition model for two-dimensional nanocrystal self-assembly on graphite. *J Phys Chem B.* 2002;106(22):5653–5658.
- [18] Zhang H, Edwards EW, Wang D, Möhwald H. Directing the self-assembly of nanocrystals beyond colloidal crystallization. *Phys Chem Chem Phys.* 2006;8(28):3288–3299.
- [19] Maillard M, Motte L, Ngo A, Pileni M. Rings and hexagons made of nanocrystals: a marangoni effect. *J Phys Chem B.* 2000;104(50):11871–11877.
- [20] Rabani E, Reichman DR, Geissler PL, Brus LE. Drying-mediated self-assembly of nanoparticles. *Nature.* 2003;426(6964):271–274.
- [21] Redl FX, Cho KS, Murray CB, O'Brien S. Three-dimensional binary superlattices of magnetic nanocrystals and semiconductor quantum dots. *Nature.* 2003;423(6943):968–971.
- [22] Nie Z, Petukhova A, Kumacheva E. Properties and emerging applications of self-assembled structures made from inorganic nanoparticles. *Nat Nanotechnol.* 2010;5(1):15–25.
- [23] Shevchenko EV, Talapin DV, Kotov NA, O'brien S, Murray CB. Structural diversity in binary nanoparticle superlattices. *Nature.* 2006;439(7072):55–59.
- [24] Min Y, Akbulut M, Kristiansen K, Golan Y, Israelachvili J. The role of interparticle and external forces in nanoparticle assembly. *Nat Mater.* 2008;7(7):527–538.
- [25] Dziomkina NV, Vancso GJ. Colloidal crystal assembly on topologically patterned templates. *Soft Matter.* 2005;1(4):265–279.
- [26] Lin X, Jaeger H, Sorensen C, Klabunde K. Formation of long-range-ordered nanocrystal superlattices on silicon nitride substrates. *J Phys Chem B.* 2001;105(17):3353–3357.
- [27] Zhang Z, Lin M. High-yield preparation of vertically aligned gold nanorod arrays via a controlled evaporation-induced self-assembly method. *J Mater Chem C.* 2014;2(23):4545–4551.
- [28] Goubet N, Richardi J, Albouy PA, Pileni MP. How to predict the growth mechanism of supracrystals from gold nanocrystals. *J Phys Chem Lett.* 2011;2(5):417–422.
- [29] Sigman MB, Saunders AE, Korgel BA. Metal nanocrystal superlattice nucleation and growth. *Langmuir.* 2004;20(3):978–983.
- [30] Guo W, Wang M, Xia W, Dai L. Evaporation-induced self-assembly of capillary cylindrical colloidal crystal in a face-centered cubic structure with controllable thickness. *J Mater Res.* 2012;27(13):1663–1671.
- [31] Strangi G, Barna V, Caputo R, De Luca A, Versace C, Scaramuzza N, Umeton C, Bartolino R, Price GN. Color-tunable organic microcavity laser array using distributed feedback. *Phys Rev Lett.* 2005;94(6):063903.
- [32] Chen J, Morris SM, Wilkinson TD, Freeman JP, Coles HJ. High speed liquid crystal over silicon display based on the flexoelectro-optic effect. *Opt Express.* 2009;17(9):7130–7137.
- [33] Sengupta A, Herminghaus S, Bahr C. Liquid crystal microfluidics: surface, elastic and viscous interactions at microscale. *Liquid Crystals Reviews.* 2014;2(2):73–110.
- [34] Tatarkova S, Burnham D, Kirby A, Love G, Terentjev E. Colloidal interactions and transport in nematic liquid crystals. *Phys Rev Lett.* 2007;98(15):157801.
- [35] Carlton RJ, Ma CD, Gupta JK, Abbott NL. Influence of specific anions on the orientational ordering of thermotropic liquid crystals at aqueous interfaces. *Langmuir.* 2012;28(35):12796–12805.
- [36] Corbett DR, Elston SJ. Modeling the helical flexoelectro-optic effect. *Phys Rev E.* 2011;84(4):041706.
- [37] De Gennes P. Calcul de la distorsion d'une structure cholesterique par un champ magnetique. *Solid State Commun.* 1968;6(3):163–165.